https://doi.org/10.5194/essd-2024-448
Preprint. Discussion started: 11 November 2024

Open Access Earth System Science Data Discussions

A high-quality Data Set for seismological studies in the East Anatolian Fault Zone, Türkiye

Leonardo Colavitti[1], Dino Bindi[2], Gabriele Tarchini[1,3], Davide Scafidi[1], Matteo Picozzi[3,4], Daniele Spallarossa[1]

[1]University of Genoa, Department of Earth, Environment and Life Sciences - DISTAV, Genoa, Italy
[2]German Research Center for Geoscience - GFZ, Potsdam, Germany
[3]National Institute of Oceanography and Applied Geophysics - OGS, Trieste, Italy
[4]University of Naples Federico II, Physics Department "Ettore Pancini", Naples, Italy

Correspondence to: Leonardo Colavitti (leonardo.colavitti@edu.unige.it)

Abstract. This work aims to develop and share a high-quality seismic dataset for the East Anatolian Fault Zone (EAFZ), which is a highly active seismic area that is prone to earthquakes, as evidenced by the two major earthquakes of magnitude 7.8 and 7.6 that occurred on February 6, 2023 in central Türkiye and northern and western Syria.

The dataset described here (available at https://doi.org/10.5281/zenodo.13838992, Colavitti et al., 2024) encompasses seismic events from January 1, 2019, to February 29, 2024, focusing on small-to-moderate earthquakes from M_L between 2.0 and 5.5 and is intended as a useful tool for researchers working on seismic source characterization and strong motion parameters.

The dataset consists of 9,442 events recorded by 271 stations and includes a total of 270,704 seismic phases (148,223 P and 122,481 S). The Complete Automatic Seismic Processor (CASP) software package ensures accurate arrival times and refined earthquake locations, while the local magnitude is calibrated using a non-parametric approach. In addition to the earthquake catalog, the dataset features strong motion parameters such as selected Peak Ground Acceleration (PGA), Peak Ground Velocity (PGV), as well as Fourier Amplitude Spectra (FAS) in the frequency range from 0.05 to 47.2 Hz.

The disseminated product aims to support applications in spectral decomposition using the Generalized Inversion Technique (GIT), promote investigations in Local Earthquake Tomography (LET) and contribute to the development of Ground Motion Prediction Equations (GMPEs). Long-term objectives include studying the spatio-temporal evolution of seismicity to identify preparatory processes for significant earthquakes, integrating this data with geodetic investigations, and enhancing earthquake hazard assessments.

https://doi.org/10.5194/essd-2024-448
Preprint. Discussion started: 11 November 2024

Open Access Earth System Science Data Discussions

1 Introduction

On February 6, 2023 a seismic sequence hit southern and central Türkiye and northern and western Syria along the East Anatolian Fault Zone (EAFZ). The sequence was started by a Mw 7.8 earthquake along the Nurdag-Pazarcık fault and followed, about 9 hours later, by a Mw 7.6 earthquake occurred north-northeast from the first shock, in Kahramanmaraş province, involving the Sürgü and Çardak faults (Güvercin et al., 2022; Dal Zilio and Ampuero, 2023; Melgar et al., 2023; Petersen et al., 2023). According to the Disaster and Emergency Management Authority (*Afet ve Acil Durum Yönetimi Başkanlığı,* AFAD), the combined death contribution in Türkiye and Syria exceeds 60,000 people, with more than 120,000 injured and an amount of economic losses of 163.6 billion USD, representing the deadliest natural disaster in the modern history of Türkiye at present, since the 526 Antioch event (Sbeinati et al., 2005).

In this study, we focus on the EAFZ, which is a portion of a major fault zone that runs through eastern Türkiye as it accommodates the tectonic relative motion between the Arabian and Anatolian microplates (Ambraseys, 1989). According to Melgar et al. (2023), the first event nucleated on a previously unmapped fault before transitioning to the East Anatolian Fault, which ruptured over a length of approximately 350 km, while the second one ruptured the Sürgü fault for ~160 km.

The goal of this study is to describe the procedure that led to the creation of a high-quality seismic dataset for the EAFZ where the 2023 Kahramanmaraş occurred and its dissemination to the scientific community in order to promote high-quality research in the seismological field. In fact, the development of high-quality datasets is fundamental for investigating critical open issues, as for instance the estimation of source parameters, such as seismic energy and stress drop, which are fundamental pieces of information for understanding fault mechanics and obtaining rupture scenarios for seismic risk mitigation, but are difficult to estimate and are affected by large uncertainties (Cotton et al., 2013; Abercrombie, 2015).

Recently, benchmark studies have been carried out to facilitate comparison of the results of different approaches to estimate source parameters applied to the same data set (e.g., Pennington et al., 2021; Morasca et al., 2022; Bindi et al. 2023a; Bindi et al. 2023b). Following these efforts, a data set for the 2019 Ridgecrest earthquake sequence was disseminated in the context of the community stress-drop validation study (Baltay et al., 2021).

We believe that the creation of high-quality, standardized and open-source seismic datasets including waveforms, Fourier Amplitude Spectra (FAS), Peak Ground Acceleration (PGA), Peak Ground Velocity (PGV), is the key to promote the progress of the seismological and seismic engineering communities. In this research, we describe in detail the procedures used to construct the dataset and the criteria applied for selecting the data to be distributed.

The dataset includes earthquakes which occurred along the EAFZ main segments (**Fig.1**) during the period from January 1, 2019 to February 29, 2024, and thus it includes both the years preceding the 2023 Kahramanmaraş earthquake and the following aftershocks.

The dataset focuses on small-to-moderate earthquakes in the magnitude range from 2.0 to 5.5, which is the typical one used in studies focusing on source parameters (Parolai et al., 2000; Parolai et al., 2007; Picozzi et al., 2017). Larger earthquakes are not included (in addition to the 2 mainshocks of the February 06, 2023, we have not considered other 22 events with magnitudes

https://doi.org/10.5194/essd-2024-448
Preprint. Discussion started: 11 November 2024

from 5.6 to 6.6), as they are already available in accelerometric databases such as the Engineering Strong-Motion Database (ESM) by Luzi et al. (2020) or in a recent work of Sandıkkaya et al. (2024).

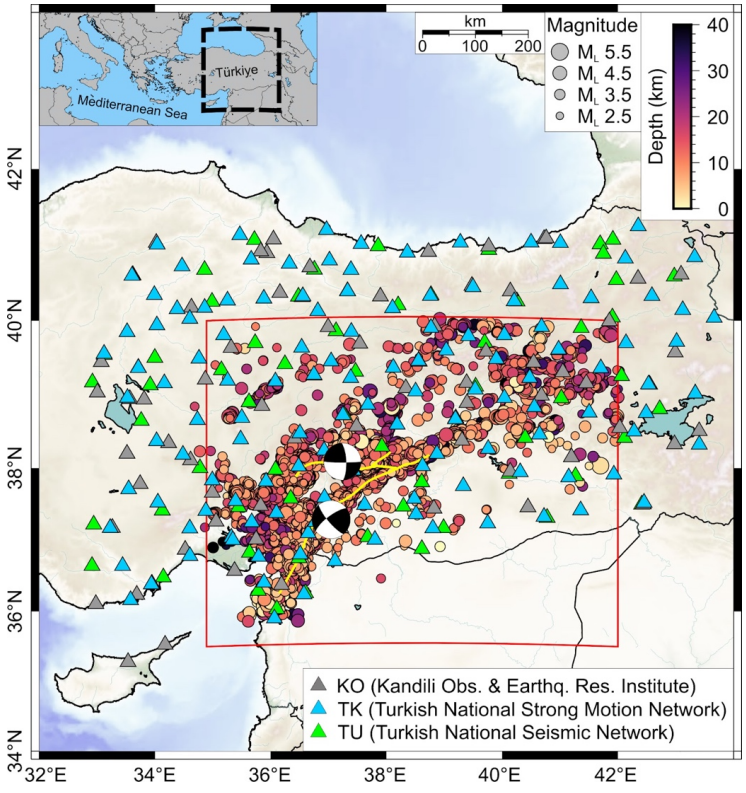

Figure 1: Dataset described in this work for the East Anatolian Fault Zone (EAFZ), delimited by the red box (Lon-Lat vertices, SW: 34.89 35.50; SE 42.00 35.50; NE 42.00 40.00; NW: 34.89 40.0). Dots represent the events with the M_L interval 2.0-5.5 in the time frame 01-01-2019 to 29-02-2024. Size is proportional to the magnitude; color palette represents the event depth. The two beach balls lying in the Melgar faults (yellow lines) represent the Mw 7.8 Pazarcık earthquake and the Mw 7.6 Elbistan earthquake occurred on February 6, 2023, which are not considered in the present catalog. The triangles show the different networks that recorded the events: KO (grey), TK (cyan) and TU (green).

The distributed dataset comprises a selected seismic catalog, selected Peak Ground Acceleration (PGA), Peak Ground Velocity (PGV), as well as selected Fourier Amplitude Spectra (FAS) within the frequency range of 0.05 to 47.20 Hz.

While the primary applications of the 2019-2024 EAFZ dataset that we envision are those discussed previously on source parameters, we believe it is particularly suitable to investigate the characteristics of the evolution of ground shaking patterns (spatial and temporal) during seismic sequences.

https://doi.org/10.5194/essd-2024-448
Preprint. Discussion started: 11 November 2024

Moreover, in the light of recent studies (Picozzi et al., 2022; Picozzi et al., 2023a; Picozzi et al., 2023b) on the spatio-temporal analysis of seismicity and ground motion parameters (i.e., GMA - Ground Motion Anomalies - defined in Picozzi et al. 2024), the provided dataset can support seismic studies for intercepting the preparatory phase of strong earthquakes.

2 Dataset construction and selection

The flowchart in **Fig. 2** shows the procedure that led to the creation and selection of the data set. We used the AFAD online catalog to geographically select all earthquakes that occurred between 32 and 44° East Longitude and 34 to 43° North Latitude (at this stage considering an area larger than the only EAFZ bounded by the red rectangle of **Fig.1**), at a depth of up to 120 km and for the period from January 1, 2019 to February 29, 2024. The initial selected reference catalog consists of 78,728 events, which are shown in the map in **Supplementary Material SM1.**

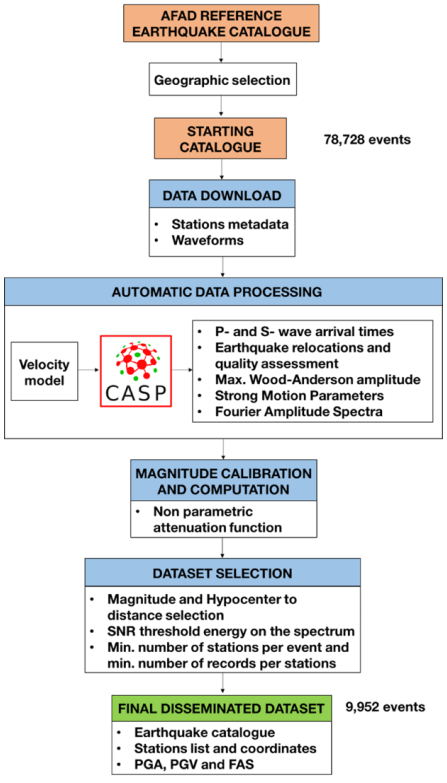

Figure 2: Flowchart of the approach adopted in this work for the construction of the dataset. Red boxes represent the catalogs of the dataset, blue boxes the main procedure of the computation. Acronym abbreviation: CASP (Complete Automatic Seismic Processor). The final box represents the disseminated dataset discussed in this work.

https://doi.org/10.5194/essd-2024-448
Preprint. Discussion started: 11 November 2024

The starting earthquakes catalog was downloaded through the web service of the International Federation of Digital Seismograph Networks (FDSN, https://www.fdsn.org/), using the *fdsnws-event* command to access event parameters via the AFAD repository (reference website: https://deprem.afad.gov.tr/event-catalog). We downloaded the metadata of the network stations belonging to the KO (Kandilli Observatory And Earthquake Research Institute, Boğaziçi University, 1971), TK (Disaster and Emergency Management Authority, 1973) and TU (Disaster and Emergency Management Authority, 1990) networks implemented in the data centers of AFAD and European Integrated Data Archive (EIDA, https://www.orfeus-eu.org/data/eida/).

All the waveforms for the three components were downloaded via the command *fdsnws-dataselect* in MiniSEED format from the EIDA and AFAD repositories. The seismograms of the events were extracted from the dataset collecting all the continuous recordings and converted in Seismic Analysis Code (SAC) format. Each time window contains 30 seconds of noise before the theoretical first arrival of P-wave and has a total duration of 90 seconds. The overall earthquake catalog containing ~78,000 events includes waveforms of different quality. While studies that focus on statistical seismology (e.g., deviations from Gutenberg-Richter law such as studies on b-value) are sometimes less sensitive to certain aspects of data quality, ensuring high data quality is critical for accurate derivation of source parameters and calibration of ground motion models, so implementing thorough data selection and quality analysis procedures is a priority.

Therefore, to generate a high-quality dataset, which is the most innovative aspect of this work, we used the Complete Automatic Seismic Processor (CASP, Scafidi et al., 2019) software, which determines seismic phase arrival times using an advanced picker engine (RSNI-Picker$_2$, see Spallarossa et al., 2014; Scafidi et al., 2016; Scafidi et al., 2018), generating a massive set of accurate P- and S-wave arrival times consistent with earthquake locations. RSNI-Picker$_2$ provides a quality estimate for each computed parameter, such as the quality weighting of the automatic picks and the standard quality parameters of the locations.

The search of reliable seismic phases arrival times in CASP is linked and driven by seismic locations. To obtain reliable seismic locations, the Non-Linear Location (NLLoc, Lomax et al., 2000; Lomax et al., 2012) algorithm was used, implementing a 1-D regional velocity model specifically suited for the East Anatolian Fault Zone (Güvercin, 2023).

As mentioned in Spallarossa et al. (2021a), CASP allows us to improve detectability, in terms of correctly detected arrival times, reliability, minimizing the rate of false picks, and, in general, the accuracy of results. The final result of the CASP procedure is a dataset of P- and S-phase arrival times and an earthquake catalog of origin time, location, depth and local magnitude M_L, all linked together.

It is worth noting that, in the initial processing phase, the local magnitudes (M_L) were calculated using a generic calibration relationship (Hutton and Boore, 1987). Subsequently, using the selected 2019-2024 EAFZ dataset after the processing with CASP, a new calibration relationship was developed using a non-parametric approach (see the Section 3.2), and the magnitudes of all events were recalculated.

https://doi.org/10.5194/essd-2024-448
Preprint. Discussion started: 11 November 2024

In this work, the automatic procedures of the CASP software also provide some strong motion parameters such as PGA, PGV and Fourier Amplitude Spectra (FAS).

The method for calculating the FAS and for the selection of the dataset is extensively described in Pacor et al. (2016) and used in subsequent studies (e.g., Picozzi et al., 2022; Castro et al., 2022a) aimed at the analysis of the seismic sequences in Central Italy. The main characteristics of the procedures used are described below.

The FAS are calculated considering 98 frequencies, equally spaced on the logarithmic scale, in the frequency range of 0.05-47.2 Hz and smoothed using the Konno and Ohmachi (1998) algorithm, where the smoothing parameter b was set to 40.

The selection of the high-quality dataset is thus carried out according to the following criteria:

(i) Events limited to the East Anatolian Fault Zone
(see red box in **Fig. 1**, Lon-Lat vertices, SW: 34.89 35.50; SE 42.00 35.50; NE 42.00 40.00; NW: 34.89 40.0);

(ii) Local magnitude M_L in the range between 2.0 and 5.5;

(iii) Hypocentral distance up to 150 km;

(iv) Recursive procedure that computes the Fourier spectra having at least 60% of points that satisfy Signal to Noise Ratio (SNR) greater than 2.5;

(v) The events are recorded by at least 6 stations and the stations have at least 6 recordings.

After the selection, the final dataset, which is ready for the distribution and whose features we will describe in the next sections, is composed of 9,442 events recorded by 271 stations (142 strong-motion sensors HN, 123 broadband seismometers with channel HH, 4 BroadBand High Gain BH and 2 short periods EH) for a total of 843,651 waveforms considering the three components of motion.

The 2019-2024 EAFZ high-quality dataset consists of an earthquake catalog, a table with the coordinates of the stations used for events recording and the strong motion parameter values, such as PGA, PGV and FAS (see section **4 – Data availability** for more details).

https://doi.org/10.5194/essd-2024-448
Preprint. Discussion started: 11 November 2024

3 Dataset characteristics

As we can observe in **Fig. 3**, the dataset is well sampled since about 50% of the earthquakes are recorded by 10 stations and about 50% of the earthquakes have more than 100 records. Further details on the distribution of number of records per event and number of records per station are shown in **SM2**.

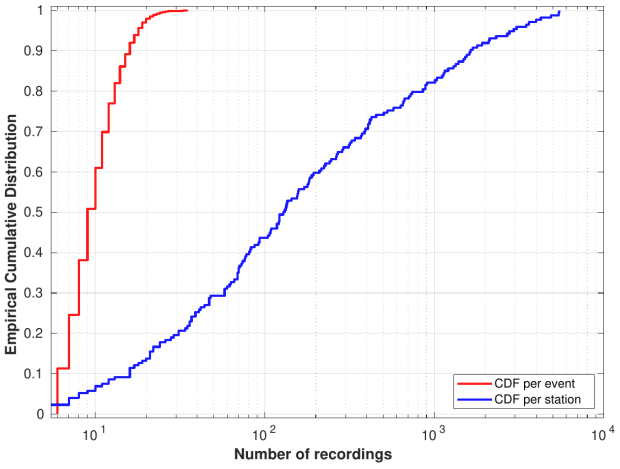

Figure 3: Cumulative Distribution Function (CDF) per event (blue) and per station (red) used in the data set.

Figure 4 represents the heatmap of the recordings with respect to hypocentral distance and local magnitude considering the sample frequency at 1 Hz (to see how the heatmap changes depending on the considered frequency, see Supplementary Material **SM3**). This figure shows as the most sampled area is around 70 km for the hypocentral distance and local magnitude around M_L 3, with some cells (with the resolution of 4 km of hypocentral distance and 0.1 of magnitude) reaching up to 300 counts.

https://doi.org/10.5194/essd-2024-448
Preprint. Discussion started: 11 November 2024

Open Access Earth System Science Data Discussions

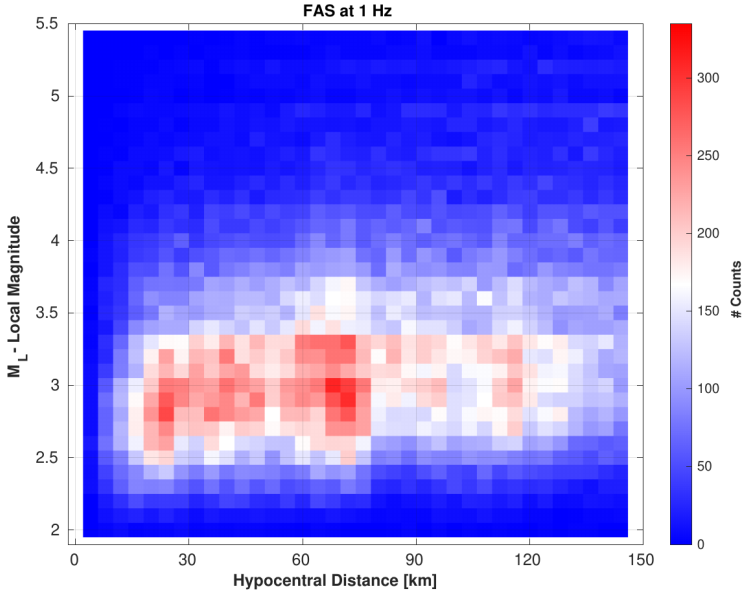

Figure 4: Local magnitude versus hypocentral distance of the recordings considered in this study at FAS = 1 Hz.

More than 50% of the records include hypocentral distance < 80 km, about 67% hypocentral distance less than 100 km and more than 80% of the data are recorded at hypocentral distance < 120 km. Regarding the magnitude distribution, about 50% of the observed recordings are below M_L 3.2, about 67% below M_L 3.5 and around 86% below M_L 4.0.

3.1 P and S Phase picking and event relocation using CASP

The event relocation is carried out by the Complete Automatic Seismic Processor procedure (CASP, from Scafidi et al., 2019). For the study area, the seismic locations are obtained using the regional 1-D velocity model of the EAFZ obtained by Local Earthquake Tomography by Güvercin (2023), which consists of 12 layers and a velocity gradient increase with depth up to Vp > 7.0 km/s at crustal depths. For detailed information about the velocity structure used as the initial model, see **SM4**. The distributed dataset has a total of 270,704 phases that were picked by CASP (see **SM 5**). **Figure 5** shows the distribution of the P and S phases.

https://doi.org/10.5194/essd-2024-448
Preprint. Discussion started: 11 November 2024

Open Access Earth System Science Data Discussions

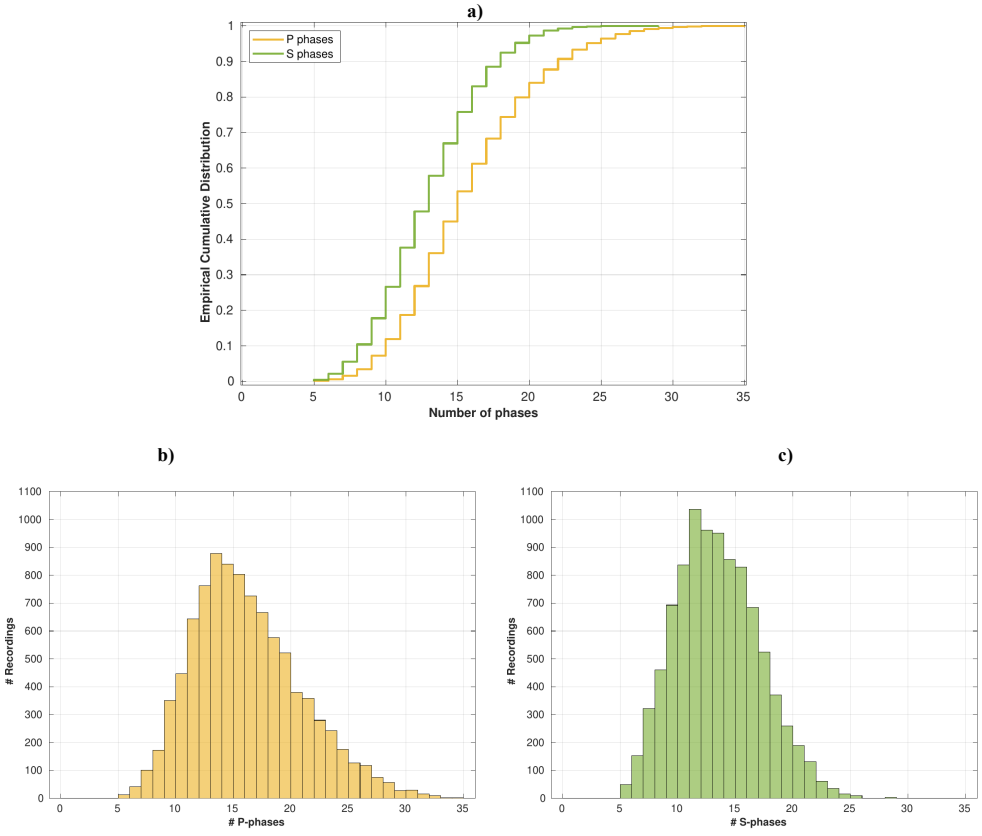

Figure 5: a) Empirical Cumulative Distribution of P and S phases in the present dataset. b) Histogram of number of P-waves, in yellow b) and S-waves, in green c) picked by the Complete Automatic Seismic Processor procedure (CASP).

The minimum number of total seismic phases recorded per event is 10 (5 for the P and 5 for the S) and, as shown in **Fig. 5a**, 50% of the entire dataset has at least 15 P-phases (yellow curve) and 13 S-phases (green curve). **Fig. 5b** and **Fig. 5c** indicates that the most frequent value in the distribution of histograms (the mode) is 13 for the P-phases and 11 for the S-phases. Overall, the P phases used are 148,223 and the S phases are 122,481 in a ratio of approximately 55% vs 45% to the total of the considered seismic phases. This considerable amount of high-precision P- and S-phase arrival times may well be exploited by the seismological community involved in tomographic studies, especially in the context of Local Earthquake Tomography (LET) investigations.

https://doi.org/10.5194/essd-2024-448
Preprint. Discussion started: 11 November 2024

3.1.1 Quality of earthquake location

The NLLoc provides us the quality and uncertainty of seismic location through several parameters, including the horizontal and depth error as shown in **Fig. 6a**, which represents the empirical curve distribution of the location error.

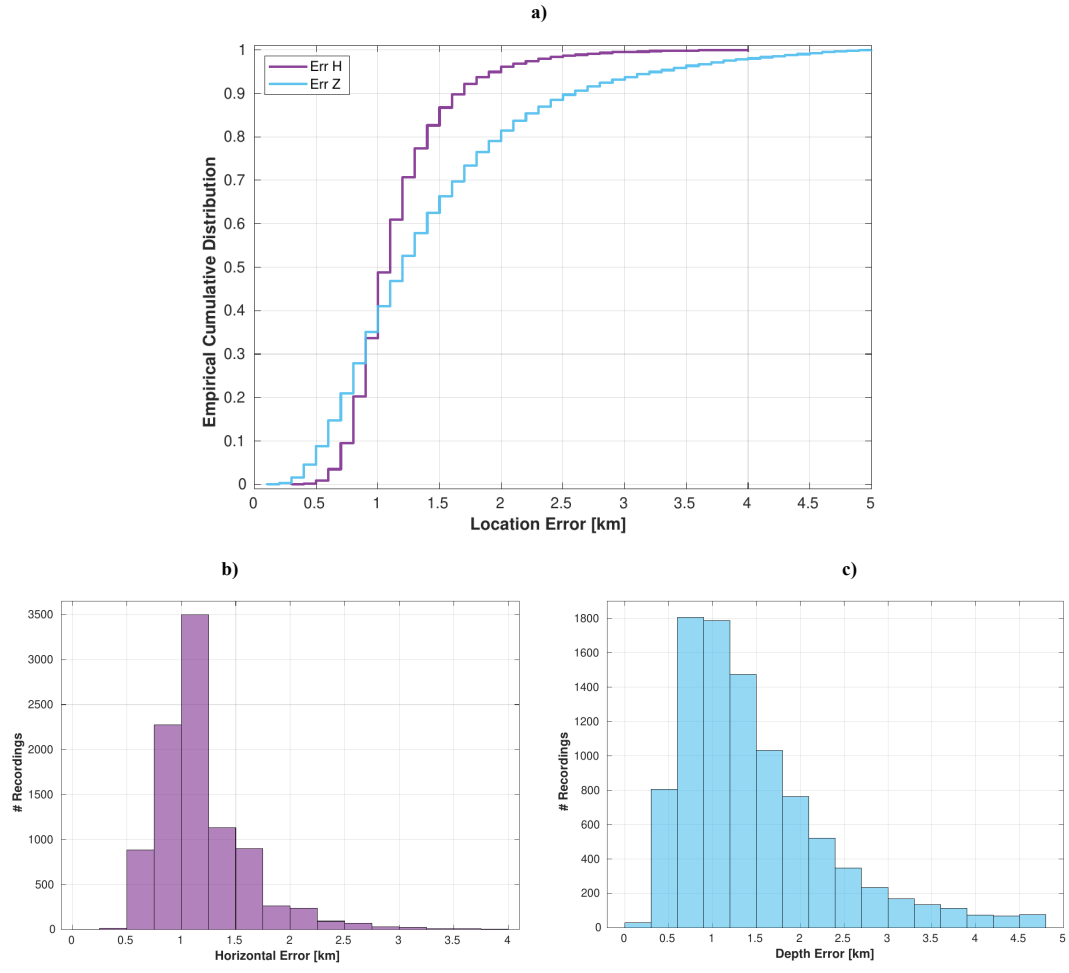

Figure 6: a) Empirical Cumulative Distribution of horizontal error and error in depth in the present dataset. b) Histogram of horizontal error (purple) and depth error (cyan) provided by the Non-Linear Location (NLLOC).

https://doi.org/10.5194/essd-2024-448
Preprint. Discussion started: 11 November 2024

The histograms concerning the error on horizontal location (**Fig. 6b**, in purple) and in depth (**Fig. 6c**, in cyan) show that the uncertainty is overall small and has a median error equal to 1.1 km for the horizontal location (min Err H: 0.30 km; max Err H: 4 km) and 1.2 km for the depth location (min Err H: 0.1 km; max Err Z: 5 km). In general, we can affirm that the NLLoc algorithm is able to find an accurate and ±1 km precise epicentral location, even in the presence of errors in crustal velocities, as observed in the work of Laporte et al. (2024), which deals with the uncertainties in earthquake location using different techniques derived from the Global Sensitivity Analysis (GSA) framework.

A further indication of the good quality of the obtained seismic location is also provided by the azimuthal gap and the Root Mean Square (RMS) error. The azimuthal gap guarantees us how well the seismic stations are distributed around the earthquake location. Approximately 98.5% of events have gaps of less than 180°, with more than 70% of the events with a gap smaller than 90° and a median for the considered events of 75° (see histogram on **SM6**).

RMS is also a key parameter for assessing the quality of earthquake location. The RMS is defined as the differences in the observed and computed arrival times of seismic waves at the stations. In formula:

$$RMS = \sqrt{\frac{1}{N}\sum_{i=1}^{N}\left(t_{obs,i} - t_{calc,i}\right)^2} \quad (1)$$

where:

- $t_{obs,i}$ is the observed arrival time at the station i;
- $t_{calc,i}$ is the computed arrival time at the station i;
- N is the total number of stations that recorded the event.

Low RMS values indicate good agreement between the observed and calculated arrival times, suggesting that the seismic location is accurate. Conversely, high RMS values indicate larger discrepancies and potential errors in the location. According to Lienert and Havskov (1995), an RMS value between 0 and 1 seconds indicates a very precise location: In the applied case (see **SM7** for details), the maximum RMS reaches a value of 0.89 seconds with a median of 0.27.

A further parameter providing indications about the reliability of seismic location in the NLLoc (Lomax, 2000) software is the covariance matrix, which is a square matrix describing the variance and covariance between residuals, and which represents a problem with 4 unknowns (spatial coordinates x and y, depth z and time t). As we can observe from the **Supplementary Material SM8**, showing histograms for covariance, the values of Cov_x and Cov_y are small, presenting a median around 0.5 (with a mean around 0.75), while higher values are reached from covariance Cov_z and Cov_t which show median values of 1.5 and 1.9 (with mean around 2.8 and 3.2, respectively).

https://doi.org/10.5194/essd-2024-448
Preprint. Discussion started: 11 November 2024

3.1.2 Depth comparison with AFAD catalog

We compared the estimates of hypocentral depth obtained with NLLoc with those from the East Anatolian Fault catalog provided by AFAD. The latter shows that the vast majority of estimates are located at about 7 km depth (i.e., 80% of the depths are between 6 and 8 km). This kind of clustering in the hypocentral depth solutions is often indicative of the presence of a high gradient in the velocity model used in the inversion procedure. This might also be the case for the AFAD catalog, as discussed by Çıvgın and Scordilis (2019).

As shown in **Fig. 7**, our study (red histogram) shows a more even distribution over different depths.

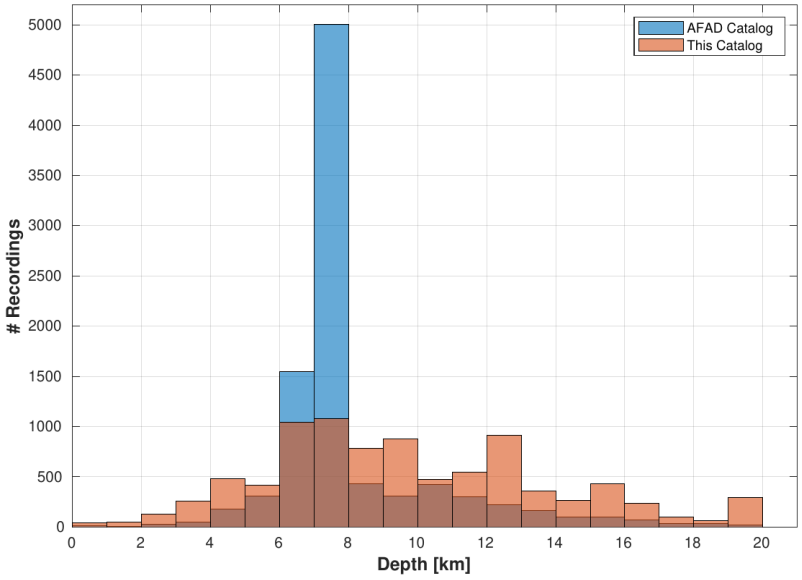

Figure 7: Depth comparison between AFAD catalog (blue) and this work (red).

The median value of the depth distribution according to this study is around 10 km depth and no particular depth distribution peaks are present. Depth estimates with a rather homogeneous distribution between 4 and 16 km seem to be consistent with the position of the complexity of fault segments that were involved in the 2023 Türkiye earthquake sequence (Gabriel et al., 2023).

https://doi.org/10.5194/essd-2024-448
Preprint. Discussion started: 11 November 2024

3.2 Magnitude computation

To obtain a homogeneous magnitude for all considered earthquakes, we calibrated a local magnitude M_L (Richter, 1935) following a non-parametric approach (Savage and Anderson, 1995; Spallarossa et al., 2002; Bindi et al., 2018; Bindi et al., 2019; Bindi et al., 2020). To determine the earthquake magnitudes, we applied the station corrections, which ensure that the amplitude measurements used for the magnitude calculation are not biased by local site effects. In our study case (see **SM9**), 2 out of 271 stations (TK.6802 and TK.6102) have a correction greater than 0.60, as they are located at sites in correspondence with terrains with low Vs,30 (less than 250 m/s). The non-parametric approach was applied to all data downloaded from the AFAD catalog.

With our analyses, we computed and provided the Wood-Anderson maximum amplitudes, which in turn were used to calibrate a EAFZ local magnitude scale according to the following equation:

$$logA_{ij}(R_{ij}) = M_{Li} + a_n logA_0(R_n) + a_{n+1} logA_0(R_{n+1}) + dM_{Lj}^C \quad (2)$$

where A_{ij} is the maximum Wood-Anderson amplitude (in millimeters) measured for event i recorded at the hypocentral distance R_{ij}. M_{Li} is the local magnitude of event i, A_0 is the zero-magnitude attenuation function defined as a table of values a_n linearly interpolated between nodes n and $n+1$, with $R_n \leq R_{ij} \leq R_{n+1}$, while dM_{Lj}^C is the magnitude correction of station j. C can be either north-south or east-west, considering the two horizontal components as independent measurements (Uhrhammer et al., 2011). As for the reference distance at which the attenuation function is anchored, we used a distance $R_{ref} = 17$ km (Hutton and Boore, 1987) and the mean value of all stations equal to zero. In Supplementary Material **SM10**, we show the output of the non-parametrically calibrated magnitude, with the comparison between the local magnitude M_L and the magnitude of the AFAD reference catalog $M_{L\,ref}$.

Figure 8 compares the calibrated $logA_0$ function performed in the EAF (listed in **Supplementary Table SM11**) with the curve computed for the California region obtained using the same approach (see Bindi et al., 2020), which is also anchored at $R_{ref} =$ 17 km.

https://doi.org/10.5194/essd-2024-448
Preprint. Discussion started: 11 November 2024

Open Access Earth System Science Data Discussions

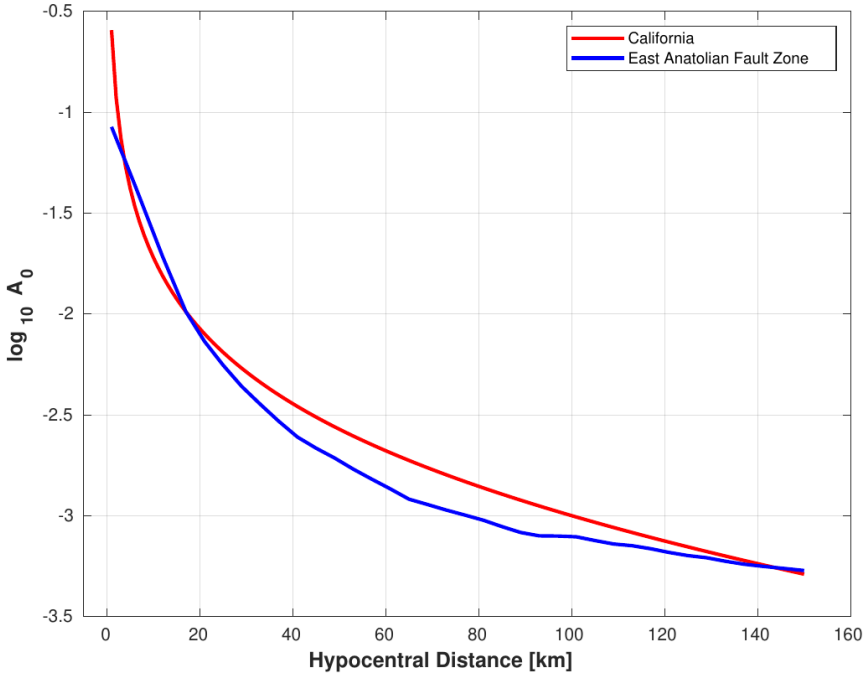

265

Figure 8: Nonparametric magnitude attenuation function logA_0 calibrated in East Anatolian Fault (blue curve) and California (red curve).

In the distance range between 20 and 100 km, the EAF curve shows a stronger attenuation than the one computed for the California region, but is similar at hypocentral distances of more than 100 km. For each value of local magnitude, the standard
270 deviation is also computed (**Fig. 9**). Both the mean and the median of the events considered are approximately 3.1, with more than 90% of the events having M_L below 4 (**Fig. 9a**).

https://doi.org/10.5194/essd-2024-448
Preprint. Discussion started: 11 November 2024

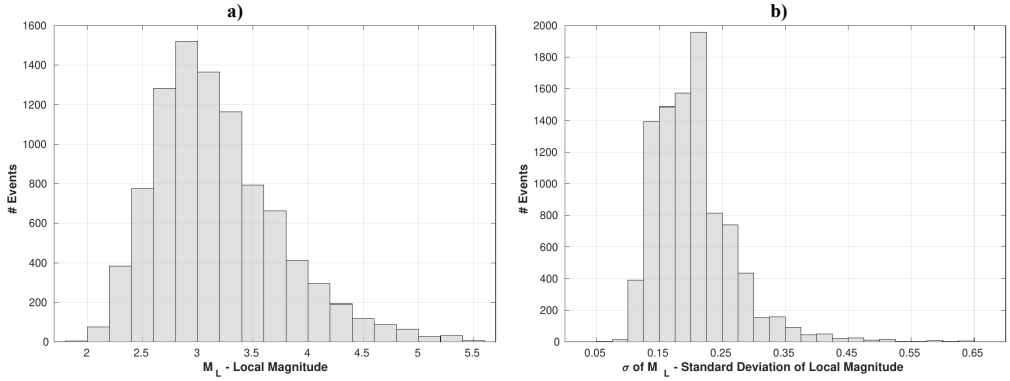

Figure 9: a) Distribution of the local magnitude a) and the standard deviation b) of the events presented in this work.

The standard deviation graph shows that the median is 0.19 (mean value 0.20) and we generally have very low values, as less than 2% of the events have magnitude values above 0.40, which shows that the local magnitude M_L measurement is very accurate.

3.1.2 Magnitude comparison with AFAD catalog

Figure 10 shows the comparison between the distribution of the local magnitude M_L of the present dataset and the distribution of the magnitude in the AFAD catalog. It is worth mentioning that the AFAD catalog does not contain a uniform parameter to characterize earthquake size, so other types of magnitudes are used in addition to the local magnitude scale, such as the duration magnitude, M_D.

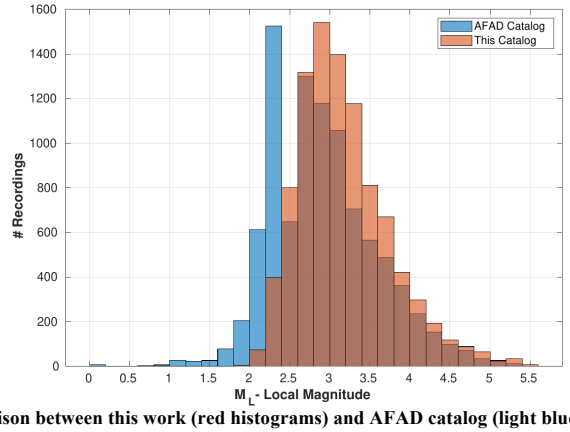

Figure 10: Magnitude comparison between this work (red histograms) and AFAD catalog (light blue histograms).

https://doi.org/10.5194/essd-2024-448
Preprint. Discussion started: 11 November 2024

The magnitude distribution seems to be quite similar between the two dataset. In the AFAD catalog, the median value is smaller (around 2.8) than that observed in our dataset, and even in this case a very small part of the distribution, about 7%, includes magnitude values above 4 (compared to 10% in our dataset).

3.3 Strong motion parameters

As mentioned before, we applied the detection of P and S onsets to estimate the local magnitude, and to extract different features from the recordings such as the peak displacement (PGD), the integral of the squared velocity IVs2 evaluated over the S-wave window at local distances, the peak ground velocity (PGV) and the peak ground acceleration (PGA). These features are extracted directly from recordings and constitute the basis of the the concept behind the Rapid Assessment of MOmeNt and Energy Service - RAMONES project (Spallarossa et al., 2021b, web page: https://distav.unige.it/rsni/ramones.php). This service provides seismic moment M0 and radiated energy Er, and relies on the measurement of specific ground motion features directly on seismograms and their correction for propagation and site effects using empirical models previously calibrated for the region of interest.

Figure 11 shows an example of a three components recording (N-S: North-South; E-W: East-West; Z: Vertical) relative to the record of the M_L 4.0 recorded at the station HASA occurred on 20 March 2023 at 15:40:34 UTC.

https://doi.org/10.5194/essd-2024-448
Preprint. Discussion started: 11 November 2024

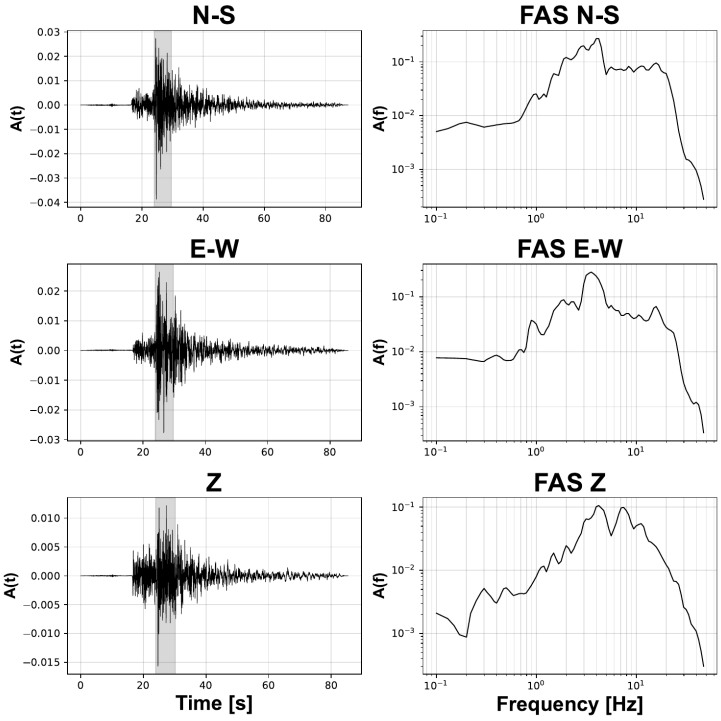

Figure 11: Record for the M_L 4.0 event occurred on 20 March 2023 at 15:40:34 UTC at the station HASA, where in gray is shown the portion of the signals for which FAS is computed. The panels on the left represent the seismic signals, on the right are the corresponding FAS. North-South component at the top, East-West component in the middle, vertical component at the bottom.

Fourier Amplitude Spectra (FAS) are calculated for the three components of the signal using a recursive procedure based on distance-dependent energy criterion to determine S-wave time window and applying a frequency-dependent threshold to the signal-to-noise ratio (in this case, SNR > 2.5) to select the spectral amplitudes for the inversion (Pacor et al., 2016). FAS are calculated on time windows starting 0.1 s before the S-wave onset and ending with 60% when the total energy of the full spectrum is reached. The spectral amplitudes are calculated considering 98 frequencies, equally spaced in the logarithmic scale, in the range between 0.05 and 47.2 Hz. In addition to the FAS dissemination, PGV and PGA values are also distributed. These values are important as they give us a complete picture of the seismic motion and the potential impact on the structures (Trifunac and Brady, 1975; Aki and Richards, 2002).

Figure 12a shows the values of $\log_{10}$PGA as a function of hypocentral distance, defined for different magnitude ranges.

https://doi.org/10.5194/essd-2024-448
Preprint. Discussion started: 11 November 2024

The solid line represents the median curve for a given magnitude, while the areas in transparency show the variability within each bin of hypocenter distance and are bounded by the lower quartile (25th percentile) and upper quartile (75th percentile), respectively.

With the PGA here we refer to the PHA (Peak Horizontal Acceleration), i.e., the composition of the horizontal components of the strong ground motion:

$$PHA = \sqrt{(PGA_{N-S})^2 + (PGA_{E-W})^2} \quad (3)$$

where PGA_{N-S} is the component of PGA along the North-South direction, while PGA_{E-W} is the component of PGA along the East-West direction.

For the distribution of all events for which PGA is available, please refer to **SM12**.

https://doi.org/10.5194/essd-2024-448
Preprint. Discussion started: 11 November 2024

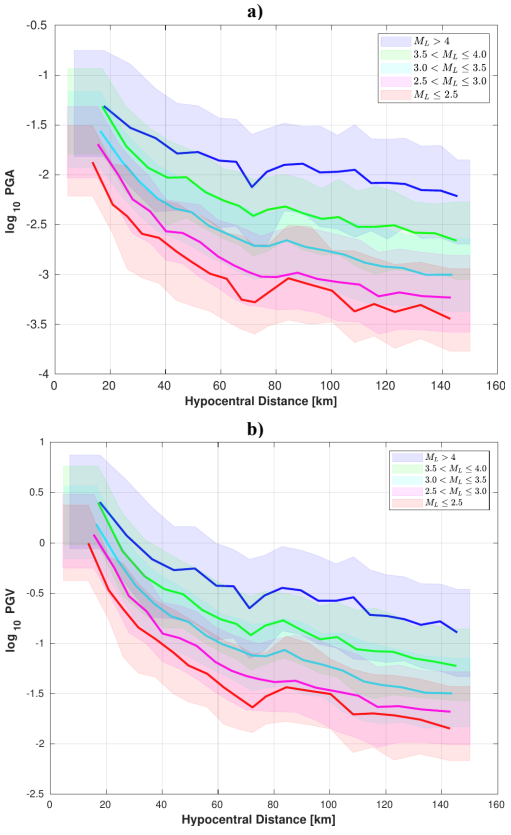

Figure 12: Distribution with hypocentral distance of the log10 PGA a) and log10 PGV b) over the S-wave window. The trends of the parameters averaged over five narrow magnitude ranges as indicated in the panels (M_L<=2.5; 2.5 < M_L <= 3; 3 < M_L <= 3.5; 3.5 < M_L <= 4.0; M_L > 4.0) are also shown. Areas in transparency show the variability of each curve bounded by the lower quartile (25th percentile) and upper quartile (75th percentile).

As was to be expected, the PGA assumes high values for small hypocentral distances and reaches median values of $\log_{10}$PGA between -2 and -1 for hypocentral distances of less than 20 km. For intermediate hypocentral distances, between 20 and 80 km, PGA values tend to decrease assuming median values of $\log_{10}$PGA between -3 and -1.5. For larger hypocentral distances, and thus beyond 80 km, $\log_{10}$PGA values seem to reach a sort of plateau. The same trend can be seen for PGV (measured in cm/s), as shown in **Fig. 12b**, with median values varying in a range where $\log_{10}$PGV is between -2 and 0.5. The curves representing the 5 magnitude ranges (red, M_L<=2.5; pink, 2.5 < M_L <= 3; cyan, 3 < M_L <= 3.5; green, 3.5 < M_L <= 4; blue > 4.0) show us that the higher the magnitude, the higher the PGA. This is particularly evident for hypocentral distances greater than 40 km, where the curves are separated as a function of magnitude.

https://doi.org/10.5194/essd-2024-448
Preprint. Discussion started: 11 November 2024

4 Data availability

The products derived by the procedures discussed above are available at the Zenodo repository: https://doi.org/10.5281/zenodo.13838992 (Colavitti et al., 2024) through tables, which are related to the events, stations, PGA and PGV files and FAS parameters In this section we thus provide a description of the tables you can find in the repository, with the explanation of the fields relative to the presented dataset.

4.1 File of earthquakes

The distributed dataset contains the following fields:

- **Id_AFAD** is the reference number of the earthquake according to AFAD
- **Date** is the date of the event (3 fields) in the format yyyy:mm:dd (years:months:days)
- **Time** is the origin time (3 fields) in the format hh:mm:ss.sss (hours:minutes:seconds)
- **Ev_Lat** is the Latitude of the earthquake in decimal degrees (°)
- **Ev_Lon** is the Longitude of the earthquake in decimal degrees (°)
- **Ev_Depth** is the depth in kilometers (km)
- **M_L** is the recalibrated local magnitude
- **StdM_L** is the standard deviation of local magnitude
- **Rms** is the root-mean-square of local magnitude residuals at maximum likelihood or expectation hypocenter, expressed in seconds (s)
- **Erh** is the horizontal error in kilometers (km), given by NLLoc algorithm
- **Erz** is the vertical error in kilometers (km), given by NLLoc algorithm
- **Gap** is the maximum azimuth gap between stations used for location, expressed in decimal degrees (°)
- **Np** is the number of P-wave phases used for location
- **Ns** is the number of S-wave phases used for location
- **Ntot** is the total number of phases, both P-wave and S-wave, used for location
- **Cov_X** is the covariance matrix value along X direction given by the NLLoc
- **Cov_Y** is the covariance matrix value along Y direction given by the NLLoc
- **Cov_Z** is the covariance matrix value along depth given by the NLLoc
- **Cov_T** is the covariance matrix related to the observed arrival times by the NLLoc

https://doi.org/10.5194/essd-2024-448
Preprint. Discussion started: 11 November 2024

4.2 File of stations

The distributed file of stations contains the following fields:

- **FDSN_Sta_Code** is the combined string code based on Network - Station - Location - Channel
- **Sta_Lat** is the latitude of the station in decimal degrees (°)
- **Sta_Lon** is the longitude of the station in decimal degrees (°)
- **Sta_Elev** is the elevation of the station in meters (m)

4.3 File of PGA and PGV

The distributed file of PGA and PGV contains the following fields:

- **Id_AFAD** is the reference number of the earthquake according to AFAD
- **FDSN_Sta_Code** is the combined string code based on Network - Station - Location - Channel
- **Dist_Hypo** is the hypocentral distance event-station in kilometers (km)
- **PGV_Z** is the Peak Ground Velocity relative to the vertical component (cm/s)
- **PGV_NS** is the Peak Ground Velocity in the N-S direction (cm/s)
- **PGV_EW** is the Peak Ground Velocity in the E-W direction (cm/s)
- **PGA_Z** is the Peak Ground Acceleration relative to the vertical component (cm/s²)
- **PGA_NS** is the Peak Ground Acceleration in the N-S direction (cm/s²)
- **PGA_EW** is the Peak Ground Acceleration in the E-W direction (cm/s²)

4.4 Files of FAS parameters

We also report the acceleration Fourier Amplitude Spectra (FAS), for 98 frequency values from 0.05 to 47.2 Hz, equally spaced on the logarithmic scale.

Each file contains the following fields:

- **Id_AFAD** is AFAD catalog reference ID
- **Ev_Lat** is the latitude of the earthquake in decimal degrees (°)
- **Ev_Lon** is the longitude of the earthquake in decimal degrees (°)
- **Depth** is the hypocentral depth in kilometers (km)
- **M_L** is the recalculated local magnitude
- **FDSN_Sta_Code** is the combined string code based on Network - Station - Location - Channel
- **Sta_Lat** is the latitude of the station in decimal degrees (°)
- **Sta_Lon** is the longitude of the station in decimal degrees (°)

https://doi.org/10.5194/essd-2024-448
Preprint. Discussion started: 11 November 2024

- **Sta_Elev** is the elevation of the station in meters (m)
- **Dist_Hypo** is the hypocentral distance event-station in kilometers (km)
- **FAS_xxx_Z** is the acceleration FAS at xxx Hz relative to the vertical component (cm/s)
- **FAS_xxx_NS** is the acceleration FAS at xxx Hz in the N-S direction (cm/s)
- **FAS_xxx_EW** is the acceleration FAS at xxx Hz the E-W direction (cm/s)

Where **xxx** refers to a frequency between 0.05 and 47.2 Hz.

The frequencies used (in Hz) are as follows: 0.05, 0.08, 0.10, 0.13, 0.15, 0.17, 0.20, 0.22, 0.25, 0.28, 0.30, 0.32, 0.35, 0.38, 0.40, 0.43, 0.45, 0.47, 0.50, 0.53, 0.56, 0.59, 0.63, 0.67, 0.71, 0.75, 0.79, 0.84, 0.89, 0.94, 1.00, 1.06, 1.12, 1.19, 1.26, 1.33, 1.41, 1.49, 1.58, 1.67, 1.77, 1.88, 1.99, 2.11, 2.23, 2.37, 2.51, 2.65, 2.81, 2.98, 3.15, 3.34, 3.54, 3.75, 3.97, 4.21, 4.46, 4.72, 5.00, 5.30, 5.61, 5.94, 6.29, 6.67, 7.06, 7.48, 7.92, 8.39, 8.89, 9.42, 9.98, 10.57, 11.19, 11.86, 12.56, 13.30, 14.09, 14.93, 15.81, 16.75, 17.74, 18.79, 19.91, 21.08, 22.33, 23.66, 25.06, 26.54, 28.12, 29.78, 31.55, 33.42, 35.40, 37.49, 39.72, 42.07, 44.56 and 47.20.

5 Conclusions

The applications and prospects of the 2019-2024 EAFZ high-quality dataset are potentially many. As we have already mentioned, one of the main applications targeted by the dataset is spectral decomposition by the Generalized Inversion Technique (GIT), which was first applied by Andrews (1986), Iwata and Irikura (1988) and Castro et al. (1990). GIT is a reliable approach for the simultaneous investigation of source, path and site in the frequency domain and plays a crucial role in improving our understanding of seismic processes and earthquake hazard assessment. This method is based on linear and time-invariant assumptions, for which the output is given by the convolution between the input and the transfer function of the system (Bindi et al., 2023b).

As we can see from **Fig. 13**, which shows the coverage map of the dataset at 1 Hz, our area is very well sampled and dense of rays, especially along the main tectonic alignments of the EAF.

https://doi.org/10.5194/essd-2024-448
Preprint. Discussion started: 11 November 2024

Open Access Earth System Science Data Discussions

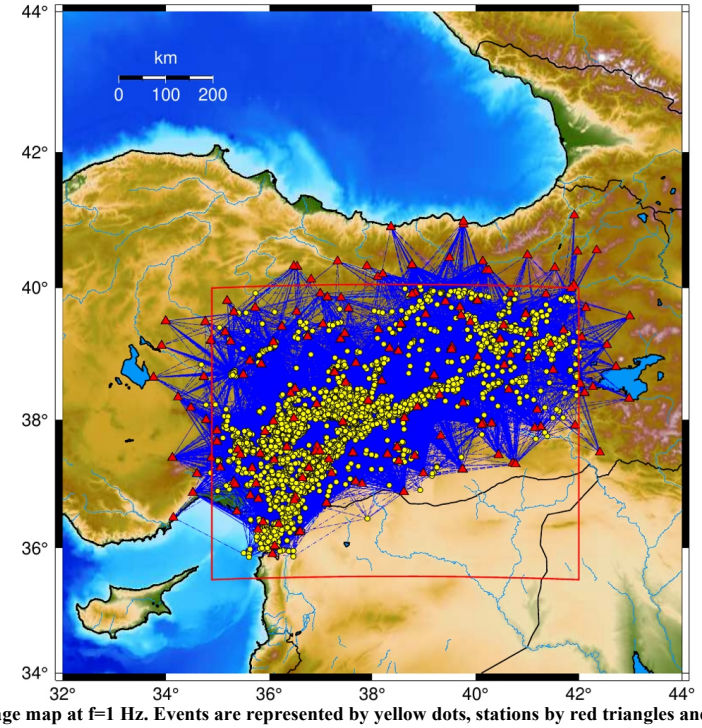

Figure 13: Ray coverage map at f=1 Hz. Events are represented by yellow dots, stations by red triangles and rays by blue lines.

One of the long-term objectives of the work is to provide a solid basis for the study of source parameters, similar to what was done for the Southern California Earthquake Center (SCEC) community, where the authors applied spectral decomposition to isolate the source spectra of some events belonging to the 2019 Ridgecrest seismic sequence (Bindi et al., 2023b) and provided epistemic analyses of the uncertainties of the results in a companion paper (Bindi et al., 2023c).

From the spatial point of view, the area is also very well sampled for the other frequencies (see **SM13** and **SM14**).

Ray coverage is crucial for the success of GIT studies as it has a direct impact on the accuracy and reliability of the derived source, path and site parameters, and ensuring comprehensive ray coverage is essential to obtain robust and meaningful results for seismological investigations.

Such dense ray coverage can also be useful to the tomography community, for example for the application of Local Earthquake Tomography (LET), that uses first arrival times (Gokalp 2012; Ozer et al., 2019; Medved et al., 2021; Güvercin, 2023), or for attenuation tomography studies (Koulakov et al., 2010; Toker and Şakir, 2022) in the East Anatolian Fault Zone or nearby areas. In this sense, the disseminated dataset can be very useful, both in terms of data quantity, in quality of earthquake location and dense frequency sampling, which can help us improve the mapping of seismic structures in such a complex geological area.

https://doi.org/10.5194/essd-2024-448
Preprint. Discussion started: 11 November 2024

The presented dataset can be an inspiration for the development of the STATION (Seismic sTATion and sIte amplificatiON, web page: https://distav.unige.it/rsni/station.php) service (Tarchini et al., 2024), which is a product based on the exchange and dissemination of seismological data using the seismic stations limited on Italian territory and in cross-border areas. Starting from an automatic picking procedure of P- and S- phases, STATION guarantees a quasi-automatic elaboration of a selection of data records and is finalized to the calculation of H/V spectral ratios and station local magnitude residuals. A similar procedure has already been started for the East Anatolian Fault using this dataset (see **SM15**), with the aim of a very precise characterization for each site considered.

Furthermore, the disseminated dataset can significantly contribute to the development of the existing Ground Motion Prediction Equations (GMPEs) in the EAFZ and thus, to some extent to the improvement of earthquake hazard assessment (Akkar and Çağnan, 2010; Kale et al., 2015).

With an available period of more than five years of seismicity, it is also possible to study the variations of the Q parameter, which represents the attenuation of seismic energy through the coda waves (Sertçelik, 2012) or, moving to higher frequencies, to contribute to the investigation of the kappa (κ) parameter, which depends on peculiar geological characteristics of the terrain (Biro, 2024). In this context, recent studies in the Central Italy region (Castro et al., 2022b; Castro et al., 2024) based on high quality datasets that include low-to-moderate seismicity (Spallarossa et al., 2022) such as the product of this work, have shown that the temporal study of κ helps to better investigate the role of fluid circulation and has provided important clues for monitoring the seismic cycle.

One of the ultimate goals for which the dataset was developed is to study the spatio-temporal evolution of seismicity to detect and verify the existence of a preparatory process for the February 6, 2023, Mw 7.8 earthquake (see Kwiatek et al., 2023; Picozzi et al., 2023b) and to understand how the identification of microseismicity is crucial for the detection and triggering of large events.

In the last few years, a set of physically based features have been developed (Picozzi et al., 2022; Picozzi et al., 2023a) aimed at intercepting the preparatory phase of strong earthquakes. In general, seismic sequences are analyzed based on the time-space distances between the earthquakes (Zaliapin et al., 2008; Zaliapin et al., 2016), which serve as an important tool in the identification of seismic crises (see **SM16**).

For a focused investigation of the spatio-temporal evolution with the aim of analyzing the systematic deviations of the peak ground acceleration generated by each earthquake from the values predicted as event-specific ground motion anomalies (eGMAs), as shown in Picozzi et al. (2024), we refer to future work dealing with this aspect in detail.

Finally, the information available in our seismological dataset may well be integrated with that deriving from geodetic investigations such as Interferometric Synthetic Aperture Radar (InSAR), which provide an image before and after the main rupture (for EAF, see An et al., 2023; He et al., 2023). These data offer the advantage of monitoring pre-, co- and post-seismic deformation and potentially identifying slow slip events.

https://doi.org/10.5194/essd-2024-448
Preprint. Discussion started: 11 November 2024

By integrating InSAR data with seismological information, it is indeed possible to gain a more comprehensive understanding of fault behavior and active tectonic mechanisms in the region, which improves the analysis of earthquake processes and helps in the assessment of seismic risk.

In summary, this work aims to produce a catalog that includes seismicity between January 1, 2019 and February 29, 2024, thus including a time window before and after the devastating February 6, 2023 sequence that struck southern and central Türkiye and northern and western Syria along the East Anatolian Fault Zone. The distributed dataset focuses on small-to-moderate earthquakes in the M_L range 2.0–5.5 and is intended in particular as a useful tool for researchers interested in seismic source characterization and strong motion parameters.

The creation of this high-quality catalog was made possible by the application of the Complete Automatic Seismic Processor - CASP (Scafidi et al., 2019) software, which allowed the identification of 270,704 seismic phases (148,223 P- and 122,481 S-wave first arrivals) for a total of 9,442 events recorded by 271 stations. All events were located with the Non-Linear Location algorithm (NLLoc, Lomax et al., 2000; Lomax et al., 2012). An initial velocity model specifically suited to the EAFZ was used, providing us with a reliable location with an uncertainty of ±1 km for both horizontal and depth location. The depth estimates we found differ from those in the AFAD reference catalog and appear to be consistent with the complexity of the fault segments involved in the 2023 Türkiye earthquake sequence. The distributed catalog also contains magnitude values (M_L) calibrated using a non-parametric approach (Bindi et al., 2020).

This dataset has been developed specifically for use in spectral decomposition, allowing for the separation and analysis of key factors such as source characteristics, attenuation and site effects. In addition, the new location provided by the dataset can provide a basis for some research investigating attenuation through the Q factor or κ parameter. Moreover, one of the long-term goals of the catalog is to understand the spatio-temporal evolution of seismicity, detecting possible proxies and intercepting the preparatory phase of strong earthquakes (Picozzi et al., 2023b).

We strongly believe that the creation of high-quality, standardized, and open-source seismic datasets, including Fourier Amplitude Spectra (FAS) and widely used strong motion parameters, such as Peak Ground Acceleration (PGA) and Peak Ground Velocity (PGV), is essential for any investigation by the seismological and earthquake engineering communities.

https://doi.org/10.5194/essd-2024-448
Preprint. Discussion started: 11 November 2024

Open Access Earth System Science Data Discussions

Code and data availability

Most of the figures were generated using MatLab software (https://mathworks.com/products/matlab.html, MathWorks, 2023). We used the Generic Mapping Tools (https://www.generic-mapping-tools.org/; Wessel et al., 2013) to produce **Figs. 1 and 13**. **Figure 11** is done through the ObsPy package (https://docs.obspy.org/; Beyreuther et al., 2010), a Python framework for processing seismological data. The dataset is freely available at the Zenodo repository: https://doi.org/10.5281/zenodo.13838992 (Colavitti et al., 2024).

Author contribution

DSp, DB and MP conceptualized the study. DSp developed the code used to compile the disseminated dataset, DB recalibrate the local magnitude. LC developed the quality checks; LC realized the images of the manuscript, with the contribution of DSc and GT.
LC organized the publication and, with the contribution of DB, GT, DSc, MP and DSp wrote the first draft of the manuscript. All authors participated to the finalization of the article.

Competing interests

The contact author has declared that none of the authors has any competing interests.

Financial support

This research is supported by the Project PREPARED "PREparatory Phase of lARge earthquakes from seismic information and gEodetic Displacement", project code 2022ZHWC9 in the frame of Bando PRIN 2022 - Progetto di Rilevante Interesse Nazionale (D. D. MUR n. 746, 31-05-2023).

https://doi.org/10.5194/essd-2024-448
Preprint. Discussion started: 11 November 2024

References

Abercrombie, R. E.: Investigating uncertainties in empirical Green's function analysis of earthquake source parameters, J. Geophys. Res. Solid Earth, 120, 4263–4277, https://doi.org/10.1002/2015JB011984, 2015.

AFAD: Disaster and Emergency Management Presidency. National Seismic Network of Turkey (DDA), International Federation of Digital Seismograph Networks available at http://tdvm.afad.gov.tr/ (last accessed February 2024).

Aki, K., and Richards, P. G. (2nd Edition): Quantitative seismology, Univ. Sci. Books, Sausalito, California, 700 pp., ISBN 0935702962, 2002.

Akkar, S., and Çağnan, Z.: A Local Ground-Motion Predictive Model for Turkey, and Its Comparison with Other Regional and Global Ground-Motion Models. Bull. Seismol. Soc. Am., 100 (6), 2978-2995, https://doi.org/10.1785/0120090367, 2010.

Ambraseys, N.: Temporary seismic quiescence: SE Turkey, Geophys. J. Int. 96(2), 11-331, https://doi.org/10.1111/j.1365-246X.1989.tb04453.x., 1989.

An, Q., Feng, G., He, L., Xiong, Z., Lu, H., Wang, X., and Wei, J.: Three-Dimensional Deformation of the 2023 Turkey Mw 7.8 and Mw 7.7 Earthquake Sequence Obtained by Fusing Optical and SAR Images, Remote Sens., 15(10), 2656, https://doi.org/10.3390/rs15102656, 2023.

Andrews, D. J.: Objective determination of source parameters and similarity of earthquakes of different size. Earthquake source mechanics, 37, 25w9-267, https://doi.org/10.1029/GM037p0259, 1986.

Baltay, A., Ide, S., Prieto, G., and Beroza, G. Variability in earthquake stress drop and apparent stress, Geophys. Res. Lett., 38(6), https://doi.org/10.1029/2011GL046698, 2011.

Beyreuther, M., Barsch, R., Krischer, L., Megies, T., Behr, Y., and Wassermann, J.: ObsPy: A Python Toolbox for Seismology, *Seismol. Res. Lett.*, 81(3), 530-533, https://doi.org/10.1785/gssrl.81.3.530, 2010.

Bindi, D., Spallarossa, D., Picozzi, M., Scafidi, D., Cotton, F.: Impact of magnitude selection on Aleatory variability associated with ground-motion prediction equations: Part I - Local, energy, and moment magnitude calibration and stress-drop variability in Central Italy, Bull. Seismol. Soc. Am., 108, 3A, 1427-1442, https://doi.org/10.1785/0120170356, 2018.

Bindi, D., Picozzi, M., Spallarossa, D., Cotton, F., Kotha, S. R.: Impact of magnitude selection on Aleatory variability associated with ground motion prediction equations: Part II - Analysis of the between-event distribution in central Italy, Bull. Seismol. Soc. Am. 109, 251-262, https://doi.org/10.1785/0120180239, 2019.

Bindi, D., Zaccarelli, R., Kotha, S. R.: Local and Moment Magnitude Analysis in the Ridgecrest Region, California: Impact on Interevent Ground-Motion Variability, Bull Seismol. Soc. Am. 111, 339-355, https://doi.org/10.1785/0120200227, 2020.

Bindi, D., Zaccarelli, R., Cotton, F., Weatherill, G., and Kotha, S. R.: Source Scaling and Ground Motion Variability along the East Anatolian Fault, The Seismic Record, 34, 311-321, https://doi.org/10.1785/0320230034, 2023a.

https://doi.org/10.5194/essd-2024-448
Preprint. Discussion started: 11 November 2024

Bindi, D., Spallarossa, D., Picozzi, M., Oth, A., Morasca, P. and Mayeda, K.: The Community Stress-Drop Validation Study - Part I: Source, Propagation, and Site Decomposition of Fourier Spectra, Seismol. Res. Lett. 94(4), 1980-1991, https://doi.org/10.1785/0220230019, 2023b.

Bindi, D., Spallarossa, D., Picozzi, M., Oth, A., Morasca, P., Mayeda, K: The Community Stress-Drop Validation Study - Part II: Uncertainties of the Source Parameters and Stress-Drop Analysis. Seismol. Res. Lett., 94 (4), 1992-2002, https://doi.org/10.1785/0220230020, 2023c.

Biro, Y.: Magnitude dependency of spectral decay parameter kappa in East Anatolian Fault related events, 18th World Conference on Earthquake Engineering, 2024.

Castro, R. R., Anderson, J. G., Singh, S. K.: Site response, attenuation and source spectra of S waves along the Guerrero, Mexico, subduction zone, Bull. Seism. Soc. Am., 80 (6A), 1481-1503, https://doi.org/10.1785/BSSA08006A1481, 1990.

Castro, R. R., Colavitti L., Vidales-Basurto, C. A., Pacor, F., Sgobba S., and Lanzano G.: Near-source attenuation and spatial variability of the spectral decay parameter kappa in central Italy, Bull. Seismol. Soc. Am., 93(4), 2299-2310, https://doi.org/10.1785/0220210276, 2022a.

Castro, R. R., Spallarossa, D., Pacor, F., Colavitti, L., Lanzano, G., Vidales-Basurto, C. A., and Sgobba, S.: Temporal variation of the spectral decay parameter kappa detected before and after the 2016 main earthquakes in central Italy, Bull. Seism. Soc. Am., 112, 3037-3045, https://doi.org/10.1785/0120220107, 2022b.

Castro, R. R., Colavitti, L., Pacor, F., Lanzano, G., Sgobba, S., and Spallarossa, D.: Temporal variation of S-wave attenuation during the 2009 L'Aquila, central Italy, seismic sequence, submitted on Geophys. J. Int., 2024.

Cıvgın, B., Scordillis, E. M.: Investigating the consistency of online earthquake catalogs of Turkey and surroundings, J. Seismol., 23, 1255-1278, https://doi.org/10.1007/s10950-019-09863-w, 2019.

Colavitti, L., Bindi, D., Tarchini, G., Scafidi, D., Picozzi, M., Spallarossa, D.: Data Set of selected strong motion parameters and Fourier Amplitude Spectra for the East Anatolian Fault Zone, Türkiye (January 2019 - February 2024) [Data set], Zenodo, https://doi.org/10.5281/zenodo.14022101, 2024.

Cotton, F., Archuleta, R., and Causse, M. What is sigma of the stress drop?, Seismol. Res. Lett., 84 (1), 42-48, https://doi.org/10.1785/0220120087, 2013.

Dal Zilio, L., and Ampuero, J. P.: Earthquake doublet in Turkey and Syria, Commun. Earth. Environ. 4, 71. https://doi.org/10.1038/s43247-023-00747-z, 2023.

Gabriel, A. A., Ulrich, T., Merchandon M., Biemiller J., Rekoske J.: 3D Dynamic Rupture Modeling of the 6 February 2023, Kahramanmaraş, Turkey Mw 7.8 and 7.7 Earthquake Doublet Using Early Observations, The Seismic Record 3(4), 342-356, https://doi.org/10.1785/032023002, 2023.

Gokalp, H.: Local earthquake tomography of the Erzincan Basin and the surrounding area in Turkey, Annals of Geophysics, 50(6), 707-724, 2007.

Güvercin, S. E., Karabulut, H., Konca, A. O., Doğan, U., and Ergintav, S.: Active seismotectonics of the East Anatolian Fault, Geophys. J. Int., 230: 50-69. https://doi.org/10.1093/gji/ggac045, 2022.

https://doi.org/10.5194/essd-2024-448
Preprint. Discussion started: 11 November 2024

Güvercin, S. E.: A local earthquake tomography on the EAF shows dipping fault structure, Turkish J. of Earth Sci. 32 (3), art. 5, https://doi.org/10.55730/1300-0985.1845, 2023.

He, L., Feng, G., Xu, W., Wang, Y., Xiong, Z., Gao, H., and Liu, X.: Coseismic kinematics of the 2023 Kahramanmaras, Turkey earthquake sequence from InSAR and optical data, Geophys. Res. Lett., 50, e2023GL104693, https://doi.org/10.1029/2023GL104693, 2023.

Hutton L. K., and Boore D. M.: The Ml scale in southern California, Bull. Seismol. Soc. Am., 77, 2074-2094, 1987.

Iwata, T., and Irikura, K.: Source parameters of the 1983 Japan Sea earthquake sequence, J. Phys. Earth 36(4), 155-184, https://doi.org/10.4294/jpe1952.36.155, 1988.

Kale, Ö, Akkar, S., Ansari, A., and Hamzehloo, H. A Ground-Motion Predictive Model for Iran and Turkey for Horizontal PGA, PGV, and 5% Damped Response Spectrum: Investigation of Possible Regional Effects. Bull. Seism. Soc. Am. 105 (2A), 963-980. https://doi.org/10.1785/0120140134, 2015.

KO - Kandilli Observatory And Earthquake Research Institute, Boğaziçi University (KOERI) [Data set]. International Federation of Digital Seismograph Networks. https://doi.org/10.7914/SN/KO, 1971.

Konno, K., and Ohmachi, T.: Ground-motion characteristics estimated from spectral ratio between horizontal and vertical components of microtremor, Bull. Seism. Soc. Am., 88 (1), 228-241, https://doi.org/10.1785/BSSA0880010228, 1998.

Koulakov, I., Bindi, D., Parolai, S., Grosser, H., and Milkereit, C.: Distribution of Seismic Velocities and Attenuation in the Crust beneath the North Anatolian Fault (Turkey) from Local Earthquake Tomography, Bull. Seism. Soc. Am., 100, 207-224, https://doi.org/10.1785/0120090105, 2010.

Kwiatek, G., Martínez-Garzón, P., Becker, D., Dresen G., Cotton F., Beroza, G., Acarel, D., Ergintav, S., and Bohnoff, M.: Months-long seismicity transients preceding the 2023 Mw 7.8 Kahramanmaraş, earthquake, Türkiye, Nature comm., 14, 7534, https://doi.org/10.1038/s41467-023-42419-8, 2023.

Laporte, M., Letort, J., Bertin, M., and Bollinger, L.: Understanding earthquake location uncertainties using global sensitivity analysis framework, Geophys. J. Int., 237(2), 1048-1060, https://doi.org/10.1093/gji/ggae093, 2024.

Lomax, A. B. and Carter, C.: Probabilistic earthquake location in 3D and layered models: introduction of a Metropolis-Gibbs method and comparison with linear locations, in Adv. in Seismic Event Location, eds. Thurber, C. H. and Rabinowitz, 101-134, Kluwer Academic Publishers, 2000.

Lomax, A., Satriano, C. and Vassallo, M.: Automatic picker developments and optimization: FilterPicker - a robust, broadband picker for real-time seismic monitoring and earthquake early warning, Seismol. Res. Lett., 83(3), 531-540, https://doi.org/10.1785/gssrl.83.3.531, 2012.

Lienert, B. R., and Havskov, J.: A Computer Program for Locating Earthquakes Both Locally and Globally, Seismol. Res. Lett., 66(5), 1995.

Luzi L., Lanzano G., Felicetta C., D'Amico M. C., Russo E., Sgobba S., Pacor, F., and ORFEUS Working Group 5, Engineering Strong Motion Database (ESM) (Version 2.0), Istituto Nazionale di Geofisica e Vulcanologia (INGV), https://doi.org/10.13127/ESM.2, 2020.

https://doi.org/10.5194/essd-2024-448
Preprint. Discussion started: 11 November 2024

MathWorks: MATLAB version 9.15 (R2023b), Natick, Massachusetts: The MathWorks Inc., 2023.

Medved, I., Polat, G., Koulakov, I.: Crustal Structure of the Eastern Anatolia Region (Turkey) Based on Seismic Tomography, Geosciences, 11, 91, https://doi.org/10.3390/geosciences11020091, 2021.

Melgar, D., Taymaz, T., Ganas, A., Crowell, B. W., Öcalan, T., Kahraman, M., Tsironi, V., Yolsal-Çevikbilen, S., Valkaniotis, S., Irmak, T. S., Eken, T., Erman, C., Özkan, Doğan, A. H., Altuntaş, C.: Sub- and super-shear ruptures during the 2023 Mw 7.8 and Mw 7.6 earthquake doublet in SE Türkiye, Seismica 2, 3, https://doi.org/10.26443/seismica.v2i3.387, 2023.

Morasca, P., Bindi, D., Mayeda, K., Roman-Nieves, J., Barno, J., Walter, W. R., and Spallarossa, D. Source scaling comparison and validation in Central Italy: data intensive direct S waves versus the sparse data coda envelope methodology, Geophys. J. Int. 231, 1573-1590, https://doi.org/10.1093/gji/ggac268, 2022.

Ozer, C., Ozyazicioglu, M., Gok, E., and Polat, O.: Imaging the Crustal Structure Throughout the East Anatolian Fault Zone, Turkey, by Local Earthquake Tomography, Pure Appl. Geophys., 176, 2235–2261, https://doi.org/10.1007/s00024-018-2076-6.

Pacor, F., Spallarossa, D., Oth, A., Luzi, L., Puglia, R., Cantore, R., Mercuri, A., D'Amico, M., and Bindi, D.: Spectral models for ground motion prediction in the L'Aquila region (central Italy): Evidence for stress-drop dependence on magnitude and depth, Geophys. J. Int., 204, 697-718, https://doi.org/10.1093/gji/ggv448, 2016.

Parolai, S., Bindi, D., Augliera, P.: Application of the Generalized Inversion Technique (GIT) to a Microzonation Study: Numerical Simulations and Comparison with Different Site-Estimation Techniques. Bull. Seismol. Soc. Am., 90(2): 286-297, 2000.

Parolai, S., Bindi, D., Durukal, E., Grosser, H., Milkereit, C.: Source Parameters and Seismic Moment-Magnitude Scaling for Northwestern Turkey. Bull. Seismol. Soc. Am., 97(2): 655-660, https://doi.org/10.1785/0120060180, 2007.

Pennington, C. N., Chen, X., Abercrombie, R. E., and Wu, Q.: Cross validation of stress drop estimates and interpretations for the 2011 Prague, OK, earthquake sequence using multiple methods, J. Geophys. Res.: Solid Earth, 126, e2020JB020888. https://doi.org/10.1029/2020JB020888, 2021.

Petersen, G. M., Büyükakpinar, P., Vera Sanhueza, F. O., Metz, M., Cesca, S., Akbayram, K., Saul, J., and Dahm, T.: The 2023 Southeast Türkiye Seismic Sequence: Rupture of a Complex Fault Network, The Seismic Record, 3(2), 134–143, https://doi.org/10.1785/0320230008, 2023.

Picozzi M., Oth A., Parolai S., Bindi D., De Landro G., and Amoroso O. Accurate estimation of seismic source parameters of induced seismicity by a combined approach of generalized inversion and genetic algorithm: Application to The Geysers geothermal area, California, J. Geophys. Res. Solid Earth, 122, 3916-3933, https://doi.org/10.1002/2016JB013690, 2017.

Picozzi, M., Spallarossa, D., Iaccarino, A. G., and Bindi, D.: Temporal evolution of radiated energy to seismic moment scaling during the preparatory phase of the Mw 6.1, 2009 L'Aquila Earthquake (Italy), Geophys. Res. Lett. 49, 7382, e2021GL097382, https://doi.org/10.1029/2021GL097382, 2022.

https://doi.org/10.5194/essd-2024-448
Preprint. Discussion started: 11 November 2024

Picozzi, M., Iaccarino, A.G., Spallarossa, D., Bindi, D.: On catching the preparatory phase of damaging earthquakes: an example from central Italy, Sci. Rep. 13, 14403, https://doi.org/10.1038/s41598-023-41625-0, 2023a.

Picozzi, M., Iaccarino, A.G., and Spallarossa, D.: The preparatory process of the 2023 Mw 7.8 Türkiye earthquake, Sci. Rep 13, 17853, https://doi.org/10.1038/s41598-023-45073-8, 2023b.

Picozzi, M., Spallarossa, D., Iaccarino A. G., and Bindi, D.: Event-specific ground motion anomalies highlight the preparatory phase of earthquakes during the 2016-2017 Italian seismicity. Comm. Earth Environ. 5, 289, https://doi.org/10.1038/s43247-024-01455-y, 2024.

Richter, C.: An instrumental earthquake magnitude scale, Bull. Seismol. Soc. Am. 25, 1-32, 1935.

Sandıkkaya, M. A., Güryuva, B., Kale, Ö., Okçu, O., İçen, A., Yenier, E., and Akkar, S.: An updated strong-motion database of Türkiye (SMD-TR), Earthq. Spectra, 40(1), 847-870, https://doi.org/10.1177/87552930231208158, 2024.

Savage, M. K., and Anderson, J. G.: A local-magnitude scale for the western great basin-eastern Sierra Nevada from synthetic Wood-Anderson seismograms, Bull. Seismol. Soc. Am. 85, 1236-1243, 1995.

Sbeinati, M. R., Darawcheh, R., and Mouty, M: The historical earthquakes of Syria: an analysis of large and moderate earthquakes from 1365 B.C. to 1900 A.D., Ann. Geophysics, 48 (3), 347-435, 2005.

Scafidi, D., Spallarossa, D., Tunino, C., Ferretti, G., Viganò, A.: Automatic P- and S-Wave Local Earthquake Tomography: Testing Performance of the Automatic Phase-Picker Engine "RSNI-Picker", Bull. Seismol. Soc. Am., 106(2), 526-536, https://doi.org/10.1785/0120150084, 2016.

Scafidi, D., Viganò, A., Ferretti, G., and Spallarossa, D.: Robust picking and accurate location with RSNI-Picker$_2$: Real-Time Automatic Monitoring of Earthquakes and Non Tectonic Events, Seism. Res. Lett., 89(4), 1478-1487, https://doi.org/10.1785/0220170206, 2018.

Scafidi, D., Spallarossa, D., Ferretti, G., Barani, S., Castello, B., and Margheriti, L.: A Complete Automatic Procedure to Compile Reliable Seismic Catalogs and Travel-Time and Strong-Motion Parameters Datasets, Seism. Res. Lett. 90(3), 1308-1317, https://doi.org/10.1785/0220180257, 2019.

Sertçelik, F.: Estimation of Coda Wave Attenuation in the East Anatolia Fault Zone, Turkey, Pure Appl. Geophys., 169, 1189-1204, https://doi.org/10.1007/s00024-011-0368-1, 2012.

Spallarossa, D., Bindi, D., Augliera, P., and Cattaneo, M.: An Ml scale in northwestern Italy, Bull. Seismol. Soc. Am. 92, 2205-2216, 2002.

Spallarossa, D., Ferretti, G., Scafidi, D., Turino, C., and Pasta, M.: Performance of the RSNI-Picker, Seismol. Res. Lett., 85(6), 1243-1254, https://doi.org/10.1785/0220130136, 2014.

Spallarossa, D., Cattaneo, M., Scafidi, D., Michele, M., Chiaraluce, L., Segou, M., and Main, I. G.: An automatically generated high-resolution earthquake catalogue for the 2016-2017 Central Italy seismic sequence, including P and S phase arrival times, Geophys. J. Int., 225, 555-571, https://doi.org/10.1093/gji/ggaa604, 2021a.

https://doi.org/10.5194/essd-2024-448
Preprint. Discussion started: 11 November 2024

Spallarossa, D., Picozzi, M., Scafidi, D., Morasca, P., Turino, C., and Bindi, D.: The RAMONES Service for Rapid Assessment of Seismic Moment and Radiated Energy in Central Italy: Concepts, Capabilities, and Future Perspectives, Seismol. Res. Lett., 92(3), 1759-1772, https://doi.org/10.1785/0220200348, 2021b.

Spallarossa D., Colavitti L., Lanzano, G., Sgobba S., Pacor F., Felicetta C.: CI-FAS_Flatfile: Parametric table of the Fourier Amplitude Spectra ordinates and associated metadata for the shallow active crustal events in Central Italy (2009-2018), [Data set], Istituto Nazionale di Geofisica e Vulcanologia (INGV), https://doi.org/10.13127/CI_dataset/CI-FAS_flatfile, 2022.

Parolai, S., Bindi, D., and Augliera, P.: Application of the Generalized Inversion Technique (GIT) to a Microzonation Study: Numerical Simulations and Comparison with Different Site-Estimation Techniques, Bull. Seismol. Soc. Am., 90(2): 286-297, 2000.

Tarchini, G., Spallarossa, D., Scafidi, D., Parolai, S., Picozzi, M., Bindi, D.: The Seismic sTATion and sIte amplificatiON service: dynamic information on Italian seismological stations, submitted on Seismol. Res. Lett., 2024, website: https://distav.unige.it/rsni/station.php.

Toker, M., and Şakir, Ş.: Upper- to mid-crustal seismic attenuation structure above the mantle wedge in East Anatolia, Turkey: Imaging crustal scale segmentation and differentiation, Physics of the Earth and Planet. Int., 329-330, 106908, 2022.

TK - Disaster and Emergency Management Authority: Turkish National Strong Motion Network [Data set]. Department of Earthquake, Disaster and Emergency Management Authority, https://doi.org/10.7914/SN/TK, 1973.

Trifunac, M., D., and Brady, A. G.: A study on the duration of strong earthquake ground motion, Bull. Seismol. Soc. Am., 65(3), 581-626, https://doi.org/10.1785/BSSA0650030581, 1975.

TU - Disaster and Emergency Management Authority: Turkish National Seismic Network [Data set]. Department of Earthquake, Disaster and Emergency Management Authority. https://doi.org/10.7914/SN/TU, 1990.

Uhrhammer, R. A., Hellweg, M., Hutton, K., Lombard, P., Walters, A. W., Hauksson, E., and Oppenheimer, D.: California Integrated Seismic Network (CISN) local magnitude determination in California and vicinity, Bull. Seismol. Soc. Am. 101, 2685-2693, https://doi.org/10.1785/0120100106, 2011.

Wessel, P., Smith, W. H. F., Scharroo, R., Luis, J., and Wobbe, F.: Generic Mapping Tools: Improved Version Released, Eos, 94, 409–410, https://doi.org/10.1002/2013EO450001, 2013.

Zaliapin I., Gabrielov, A., Keilis-Borok, V., and Wong, H.: Clustering analysis of seismicity and aftershock identification, Phys. Rev. Lett, https://doi.org/10.1103/PhysRevLett.101.018501, 2008.

Zaliapin, I., and Ben-Zion, Y.: A global classification and characterization of earthquake clusters, Geophys. J. Int. 207, 608-634, https://doi.org/10.1093/gji/ggw300, 2016.